26.—Effect of Some Impurities on the Pressure-sintering of Alumina

By G. M. Fryer

*Houldsworth School of Applied Science, University of Leeds**

ABSTRACT E137/C525

Pressure-sintering experiments are described, from which were obtained activation energies for ionic diffusion in un-doped alumina, and in alumina doped with either magnesia or tantalum pentoxide. The thermodynamics of vacancy formation in alumina have been examined, and six theoretical activation energies for diffusion have been calculated using the three measured values. The calculated activation energies have been correlated with published values for tracer diffusion in alumina. Calculations of diffusion coefficients from the pressure-sintering work show satisfactory agreement with published tracer diffusion coefficients.

Effet de quelques impuretés sur le frittage sous pression de l'alumine

L'auteur décrit des expériences de frittage sous pression qui ont conduit à des énergies d'activation pour la diffusion ionique dans l'alumine non dopée et dans l'alumine dopée soit avec de la magnésie, soit avec du pentoxyde de tantale. Les aspets thermodynamiques de la formation de vacances dans l'alumine sont examinés et six énergies d'activation théoriques sont calculées pour la diffusion à l'aide des trois valeurs mesurées. Les énergies d'activation calculées sont comparées aux valeurs publiées pour la diffusion de traceurs dans l'alumine. Les calculs de coefficients de diffusion, basés sur le frittage sous pression effectué en pratique, fournissent des résultats qui concordent de façon satisfaisante avec les coefficients publiés pour la diffusion des traceurs.

Einflüße einiger Verunreinigungen auf das Drucksintern von Aluminiumoxid

Experimente über Drucksinterung werden beschrieben, aus denen die Aktivierungsenergien der Ionendiffusion in undotiertem Aluminiumoxid und in solchem, das mit Magnesiumoxid oder Tantalpentoxid dotiert war, ermittelt wurden. Die Thermodynamik der Leerstellenbildung in Aluminiumoxid wurde untersucht und es ließen sich sechs theoretische Diffusionsaktivierungsenergien unter Benutzung der drei gemessenen Werte berechnen. Die berechneten Aktivierungsenergien wurden mit Literaturwerten der Tracer-Diffusion in Aluminiumoxid in Beziehung gesetzt. Die Berechnung der Diffusionskoeffizienten aus den Drucksinter-Versuchen zeigen befriedigende Übereinstimmung mit den aus der Literatur bekannten Tracer-Diffusionskoeffizienten.

1. INTRODUCTION

It has been shown elsewhere[1] that the shrinkage of an alumina polycrystal during the final stages of pressure-sintering is well described by the equation

$$\frac{1}{V_s}\frac{\mathrm{d}V}{\mathrm{d}t} = -Z\frac{\sigma}{l^2}\frac{D_M\Omega_s}{kT}\left(\frac{P}{\rho}\right)^{\frac{1}{3}} \quad . \quad . \quad . \quad (1)$$

or

$$\left(\frac{\rho}{P}\right)^{\frac{1}{3}} = \frac{2}{3}\frac{Z\sigma}{l^2}\frac{D_M\Omega_s}{kT}t + \text{constant} \quad . \quad . \quad (2)$$

where V_s is the volume of solid material, $\mathrm{d}V/\mathrm{d}t$ is the rate of volume change of the compact, σ is the applied pressure, l is the mean pore separation, D_M is the effective "molecular" diffusion coefficient, Ω_s is the volume of a "molecule" of the crystal, k is Boltzmann's constant, T is the absolute temperature, P is the fractional porosity and ρ the relative density ($P = 1-\rho$). Z is a constant of proportionality, which must be evaluated before the equation may be used to determine diffusion coefficients. The effective "molecular" diffusion coefficient is defined by the relationships:[2]

$$D_M = -(D_T)_a\left(\frac{1+z_a-z_c}{f_a z_c}\right), \text{ if } (D_T)_c \gg (D_T)_a \quad (3a)$$

or

$$D_M = (D_T)_c\left(\frac{1+z_a-z_c}{f_c z_a}\right), \text{ if } (D_T)_a \gg (D_T)_c \quad . \quad (3b)$$

where the subscripts a and c refer to anions and cations respectively, D_T is the tracer diffusion coefficient, z is the ionic charge expressed as a multiple of the charge on the electron, and f is the jump correlation factor. D_M can be expressed as $D_0 \exp(-Q/RT)$, where D_0 is a constant, Q is an activation energy, and R is the gas constant per gram molecule. The present paper describes experiments undertaken to determine the values of Q and D_0, firstly in compacts of undoped alumina, and then in compacts doped with impurities chosen for their effect on the vacancy equilibrium in alumina.

2. APPARATUS

The pressure-sintering apparatus has been fully described elsewhere.[1] The alumina powder (Linde A nominal particle size 0·3 μm) was pressed in a graphite die with a 9·5 mm bore, enclosed within a sintered-alumina vacuum envelope tube. This in turn was surrounded by a multi-element molybdenum-in-alumina furnace, the temperature of which could be controlled to within one or two degrees centigrade of the set value by

*Now at the Department of Ceramics with Refractories Technology, The University of Sheffield.

means of a proportional controller system. Constant loads could be applied to the die plunger by means of a weighted lever, and plunger displacement could be measured at any time during an experiment using a sensitive dial gauge.

3. EVALUATION OF THE CONSTANT Z

A value of the constant Z in Equations (1) and (2) is required before diffusion coefficients can be evaluated from pressure-sintering shrinkage data.

An attempt was made to estimate Z by assuming that the compact contained equal-sized equally-spaced pores, and that the average length of the vacancy diffusion path was about one quarter the pore separation. Using these assumptions, a value $Z \sim 20$ was obtained, but tentative evaluations of diffusion coefficients from some of the experimental data yielded values several orders of magnitude higher than tracer diffusion coefficients. It was therefore decided to evaluate Z by comparison with the geometrical constant in the Nabarro–Herring creep equation, by obtaining creep data with a pressure-sintered sample.

3.1 Experimental Procedure

A compact of Linde A alumina was pressed at 1304°C with an applied pressure of 5000 lb. in^{-2}, shrinkage data being obtained throughout the experiment. After the compact had cooled, its density was measured by weighing in air and in alcohol, so that the density at any time during shrinkage could be calculated. The pressing time was $7\frac{1}{2}$ h, and the pellet produced was 3·19 mm thick, 9·595 mm diam., with a relative density of 0·990. A plot of $(\rho/P)^{\frac{1}{3}}$ *versus* time (cf. Equation (2)) was a straight line of gradient $3{\cdot}25 \pm 0{\cdot}15$ h^{-1}.

The pellet was then inserted in a modified die, arranged so that it would experience no lateral constraint during pressing. The assembly was placed within the pressure-sintering apparatus and the temperature was raised to the value used previously for compacting the pellet (1304°C). After 1 h at this temperature, to allow the apparatus to attain thermal equilibrium, a pressure of 5000 lb.in^{-2} was again applied to the plunger, and the change in length of the pellet was recorded during the following $3\frac{1}{2}$ h. Because of the absence of restraint on the sides of the pellet, the observed deformation was presumably the result of Nabarro–Herring creep under a uniaxial compressive stress: this mechanism has been confirmed consistently for stressed dense alumina.[3,4,5] The observed strain rate was 5.10^{-3} h^{-1}.

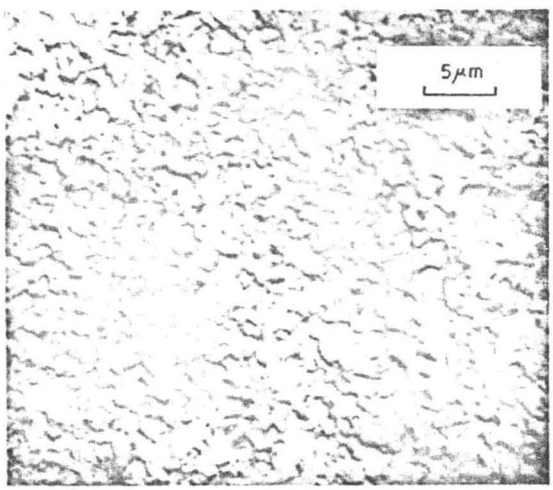

FIGURE 1
Etched section of pressure-sintered specimen used for creep experiment.

On completion of the creep experiment the pellet was sectioned and polished (using 6-μm and 1-μm diamond paste on successive lead laps). The diffraction patterns generated by pores lying below the polished surface were then sought using reflected light with a ×140 oil-immersion microscope objective. The pore separation was estimated to be 1 μm approximately.

The polished surface of the specimen was then etched in orthophosphoric acid (30 sec. at 300°C) and examined microscopically (×3000 magnification, reflected light). The etched grain boundaries were easily distinguished (Figure 1), and the grain size was estimated to be about 1·5 μm.

3.2 Results

From Equation (2),

$$\frac{\mathrm{d}}{\mathrm{d}t}\left(\frac{\rho}{P}\right)^{\frac{1}{3}} = \frac{2}{3}\frac{Z\sigma}{l^2}\frac{D_M\Omega_s}{kT} \quad . \quad . \quad . \quad (4)$$

The theory of Nabarro–Herring creep, re-written as applying to a binary ionic polycrystal, predicts that the strain rate

$$\dot{\epsilon} = \frac{40}{3}\frac{D_M\Omega_s}{kT}\frac{\sigma}{L^2} \quad . \quad . \quad . \quad (5)$$

where L is the grain size. In the case where $\mathrm{d}/\mathrm{d}t\ (\rho/P)^{\frac{1}{3}}$ and $\dot{\epsilon}$ are measured under similar conditions of temperature and pressure, as in the present experiment, Equations (4) and (5) can be combined to give

$$Z = \frac{20}{\dot{\epsilon}}\left(\frac{l}{L}\right)^2 \frac{\mathrm{d}}{\mathrm{d}t}\left(\frac{\rho}{P}\right)^{\frac{1}{3}}$$

so that, by inserting the appropriate values for the various quantities, as obtained in the present experiment, one obtains

$$Z = 6(\pm 3)\,10^3$$

where the uncertainty is caused mainly by the uncertainties in l and L.

This experimentally-determined value of Z is unexpectedly high, and implies that the vacancies migrating from the pore surfaces follow very short diffusion paths. Because a given grain boundary must receive an equal flux of vacancies over all parts of its area if it is to collapse uniformly, it is further implied that a major part of the total vacancy flux within the pressed compact does not originate at pore surfaces. In other words, it seems possible that pellet shrinkage during pressure-sintering is greatly enhanced by change of grain shape by Nabarro–Herring creep (or by grain-boundary diffusion). The pore surfaces, however, are the only net source of vacancies, so that the shrinkage rate must be governed by the total pore surface area within the compact. The arguments leading to Equation (1) thus remain valid.

Equation (2) may now be re-written

$$\left(\frac{\rho}{P}\right)^{\frac{1}{3}} = 4\ (\pm 2)\ 10^3 \frac{\sigma}{l^2} \frac{D_M \Omega_s}{kT} t + \text{constant} \quad . \quad (6)$$

4. TEMPERATURE DEPENDENCE OF SHRINKAGE RATE

4.1 Experimental Procedure

It has been reported elsewhere [1] that the gradient of a plot of $(\rho/P)^{\frac{1}{3}}$ *versus* time for an alumina compact during pressure-sintering is usually constant, in accordance with Equation (2), over a range of relative densities extending from $<0{\cdot}90$ to about 0·96. (Outside these limits the gradient was usually again constant, but with slightly different values from that of the main part of the plot, presumably because of changes in pore geometry). However, it was also observed that these gradients could vary considerably amongst different specimens even though the same experimental conditions were used in each case, presumably because of minor differences in pore separation. For this reason it was considered that the effect of a change of temperature on densification rate could not easily be evaluated by comparing the shrinkage rates of different specimens.

The method adopted was to observe the shrinkage of a compact at a given temperature while 2–3% densification took place, and then to lower the temperature by about 50°C and measure the new shrinkage rate.

The detailed procedure was as follows. The alumina powder was inserted in the die and outgassed (under vacuum) for about 12 h at about 350°C. The temperature was then raised to the required value with a pressure of 5000 lb.in^{-2} applied to the compact, after which the load was reduced or removed so that little or no further densification occurred during the hour or more required for the apparatus to reach thermal equilibrium. A suitable load (sufficient to cause a reasonable shrinkage rate at the chosen temperature) was then applied, and the shrinkage of the compact was plotted against time until an estimated density change of 2–3% had been accomplished. At this time the temperature was reduced to a new value about 50°C lower, and the new shrinkage curve was plotted. The general shape of the plot is shown diagrammatically in Figure 2A, the temperature being reduced at point A. The part of the curve immediately following point A represents a combination of compact shrinkage and thermal contraction, eventually becoming a pure shrinkage curve at point B, about 40 min. later. The extent of the thermal contraction was of course unknown, and until it had been evaluated the true pellet lengths represented by the part of the plot prior to point A could not be calculated from the final length of the pellet. To evaluate the amount of the thermal contraction, the pellet was permitted to shrink until the density reached was sufficiently high for the shrinkage rate to have become negligible (point C in Figure 2A). The temperature was then again raised to its initial value, and the amount of thermal expansion evaluated by subtracting the apparent length at C from that at D (about 40 min. later). When the apparatus had been allowed to cool to room temperature, the pellet was removed and its length and density measured. The plot of $(\rho/P)^{\frac{1}{3}}$ *versus* time for such an experiment possessed the shape shown diagrammatically in Figure 2B. The activation energy for diffusion could be calculated from the gradients of the two parts of the latter plot, using the relationship

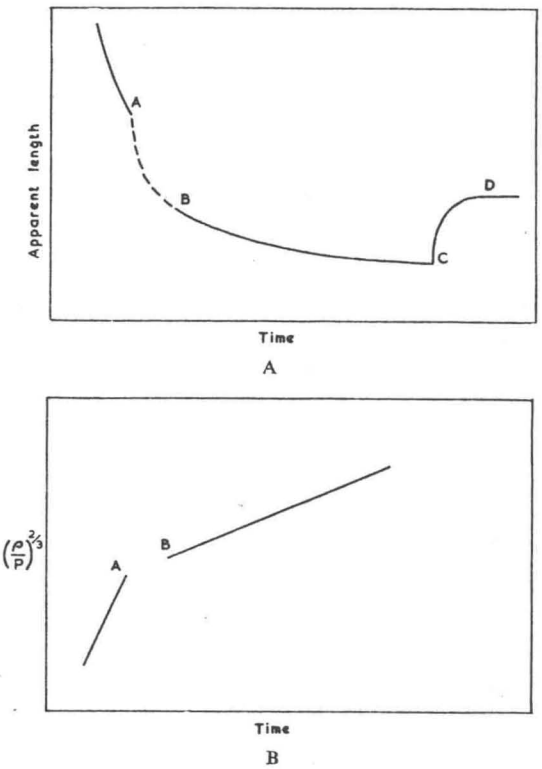

FIGURE 2

Schematic shape of:

A. Shrinkage plots obtained during temperature-dependence experiments.

B. Plot of densification-data corresponding to shrinkage plot in A.

$$Q = R\left(\frac{T_1 T_2}{T_1 - T_2}\right) \ln \left(\frac{S_1 T_1}{S_2 T_2}\right)$$

where S_1 and S_2 are the gradients of the plot of $(\rho/P)^{\frac{1}{3}}$ against time, at temperatures T_1 and T_2 (°K) respectively.

4.2 Experiments with Undoped Alumina

The first experiments in the series were performed using untreated Linde A alumina. Four satisfactory sets of results (in which both parts of the shrinkage plot were obtained at relative densities lower than 0·96) were obtained using four different pairs of temperatures. Details are given in Table 1 and plots of $(\rho/P)^{\frac{1}{3}}$ against time for two of them are shown, as an example of the type of plot obtained, in Figure 3.

The value of the activation energy for diffusion is seen to be 115($\pm$4) kcal.mole^{-1}. The quoted uncertainty arises mainly because of the degree of precision with which the temperature could be measured.

4.3 Experiments with Magnesia-doped Specimens

Magnesium was chosen as a doping cation because it possesses a lower valency than that of aluminium, and so small amounts in solid solution in alumina may be expected to cause an excess concentration of oxygen

Table 1

	Stress ($lb.in^{-2}$)	Temperature (°K)	$\frac{d}{dt}\left(\frac{\rho}{P}\right)^{\frac{2}{3}}$ (h^{-1})	Q ($kcal.mole^{-1}$)
1	5000	1581 1527	2·36 0·66	116 ± 4
2	4000	1634 1581	2·42 0·75	117 ± 4
3	3000	1684 1634	4·24 1·54	114 ± 4
4	5000	1527 1473	0·66 0·167	116 ± 4

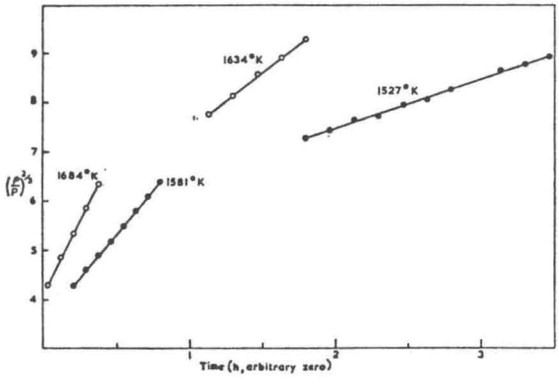

FIGURE 3
Examples of densification-data plots obtained during temperature-dependence experiments.

vacancies. This consideration will be examined more closely in a later section.

Measured quantities of magnesia were added to Linde A alumina by mixing the two powders while in suspension in alcohol. The alcohol was then removed by evaporation.

A first set of experiments was performed using a mixture containing 0·25$^{w}/_{o}$ of magnesia, but the results obtained were very erratic, with apparent activation energies ranging between 37 and 116 kcal.mole^{-1}. It was considered possible that, in the presence of excess magnesium ions at the grain boundaries, the concentration of magnesium within the crystals might be varying with temperature, or else that the results were being affected by the formation of spinel.

A second set of five experiments using alumina containing 0·025$^{w}/_{o}$ of magnesia was then performed. This time, consistent values of activation energy were obtained over a temperature range from 1469 to 1668°K. The results are summarized in Table 2. It is seen that the addition of magnesium caused the activation energy for diffusion to be increased from 115 to 130 kcal.mole^{-1}.

4.4 Experiments with Specimens containing Tantalum Pentoxide.

Tantalum was chosen as a doping cation because its valency (+5) is higher than that of aluminium, and an excess concentration of aluminium vacancies will be expected to exist in an alumina lattice containing this impurity. This consideration will be examined more fully in a later section.

Table 2

	Stress ($lb.in^{-2}$)	Temperature (°K)	$\frac{d}{dt}\left(\frac{\rho}{P}\right)^{\frac{2}{3}}$ (h^{-1})	Q ($kcal.mole^{-1}$)
5	4000	1577 1523	3·32 0·76	130 ± 6
6	2000	1668 1617	1·98 0·60	129 ± 5
7	5000	1539 1482	1·47 0·30	129 ± 5
8	2000	1665 1617	1·36 0·44	129 ± 5
9	5000	1523 1469	1·44 0·305	133 ± 6

It was not known for certain whether tantalum would enter the corundum lattice, nor was the most satisfactory method of doping the alumina specimens known, but it was decided that a first attempt would be made by mixing the oxide powders while in suspension in alcohol.

The tantalum pentoxide was first ground with an alumina pestle and mortar. The ground powder was then stirred into a beaker of alcohol and allowed to settle for 10 min. The alcohol, containing the oxide particles sufficiently fine to stay in suspension, was then decanted, and the oxide was recovered by permitting the alcohol to evaporate. A weighed amount of this selected oxide was then mixed with alumina powder whilst in suspension in alcohol, to give a mixture containing 0·125$^{w}/_{o}$ of tantalum pentoxide. This percentage was chosen so that the molecular concentration of Ta_2O_5 in the alumina would be similar to that of MgO in the specimens containing 0·025$^{w}/_{o}$ (Section 4.3).

Shrinkage rates at three pairs of temperatures were measured; the results are summarized in Table 3.

Table 3

	Stress ($lb.in^{-2}$)	Temperature (°K)	$\frac{d}{dt}\left(\frac{\rho}{P}\right)^{\frac{2}{3}}$ (h^{-1})	Q ($kcal.mole^{-1}$)
10	4000	1577 1509	2·15 0·27	147 ± 10
11	3000	1655 1590	2·0 0·34	145 ± 10
12	4000	1617 1563	2·64 0·52	154 ± 10

It is seen that the addition of tantalum pentoxide caused the activation energy for diffusion to be increased from about 115 kcal.mole^{-1} for undoped alumina to about 150 kcal.mole^{-1}. So marked a change in the diffusion kinetics was taken to confirm that the tantalum pentoxide had been able to enter the corundum lattice.

5. DIFFUSION COEFFICIENTS

Effective "molecular" diffusion coefficients may be calculated from the re-arranged form of Equation (6)

$$D_M = 3(\pm 2)\,10^{-4}\,\frac{l^2 kT}{\sigma\Omega_s}\,\frac{d}{dt}\left(\frac{\rho}{P}\right)^{\frac{2}{3}}$$

Table 2

re	$\frac{d}{dt}\left(\frac{\rho}{P}\right)^{\frac{1}{3}}$ (h^{-1})	Q (kcal.mole^{-1})
	3·32 0·76	130 ± 6
	1·98 0·60	129 ± 5
	1·47 0·30	129 ± 5
	1·36 0·44	129 ± 5
	1·44 0·305	133 ± 6

certain whether tantalum would
tice, nor was the most satis-
g the alumina specimens known,
first attempt would be made by
s while in suspension in alcohol.
e was first ground with an alum-
e ground powder was then stirred
and allowed to settle for 10 min.
the oxide particles sufficiently
n, was then decanted, and the
permitting the alcohol to evapo-
of this selected oxide was then
owder whilst in suspension in
re containing 0·125% of tant-
rcentage was chosen so that the
of Ta_2O_5 in the alumina would
gO in the specimens containing

ree pairs of temperatures were
summarized in Table 3.

Table 3

re	$\frac{d}{dt}\left(\frac{\rho}{P}\right)^{\frac{1}{3}}$ (h^{-1})	Q (kcal.mole^{-1})
	2·15 0·27	147 ± 10
	2·0 0·34	145 ± 10
	2·64 0·52	154 ± 10

addition of tantalum pentoxide
ergy for diffusion to be increased
nole^{-1} for undoped alumina to
So marked a change in the dif-
en to confirm that the tantalum
e to enter the corundum lattice.

ON COEFFICIENTS

" diffusion coefficients may be
ranged form of Equation (6)

$$10^{-4}\,\frac{l^2kT}{\sigma\Omega_s}\,\frac{d}{dt}\left(\frac{\rho}{P}\right)^{\frac{1}{3}}$$

while the pre-exponential factor D_0 is given by

$$D_0 = D_M \exp(Q/RT)$$

The pore separation for one specimen of undoped alumina, i.e. that used during the determination of the factor Z (Section 3), was already known. Two further specimens, one doped with magnesia and the other with tantalum pentoxide, were examined microscopically by the methods described in Section 3, and were both found to possess pore separations of about 1 μm and grain sizes 1–2 μm. The two specimens were those referred to as 5 and 11 in Tables 2 and 3. For all three specimens, therefore, l was about 10^{-4} cm, while Ω_s (the volume of a complete "molecule" of alumina) was taken as being $4{\cdot}2.10^{-23}$cm^3 (calculated from the theoretical density of alumina and the atomic weights of the constituent ions). The values of D_M and D_0 could then be calculated: the results are shown in Table 4.

The three derived values of D_M are plotted on Figure 4, and through them are drawn lines (Plots A, B and C)

Table 4

Specimen	*Additive*	$\frac{d}{dt}\left(\frac{\rho}{P}\right)^{\frac{1}{3}}$ (h^{-1})	*Pressure* (dynes cm^{-2})	*Temperature* (°K)	D_M (cm^{2}sec^{-1}) (±70%)	D_0 (cm^{2}sec^{-1}) (±70%)
Z specimen	None	3·25	$3{\cdot}5\ 10^8$	1577	$4{\cdot}0\ 10^{-14}$	$3{\cdot}3\ 10^2$
5	MgO	3·32	$2{\cdot}8\ 10^8$	1577	$5{\cdot}1\ 10^{-14}$	$3{\cdot}8\ 10^4$
11	Ta_2O_5	2·0	$2{\cdot}1\ 10^8$	1655	$4{\cdot}3\ 10^{-14}$	$2{\cdot}7\ 10^6$

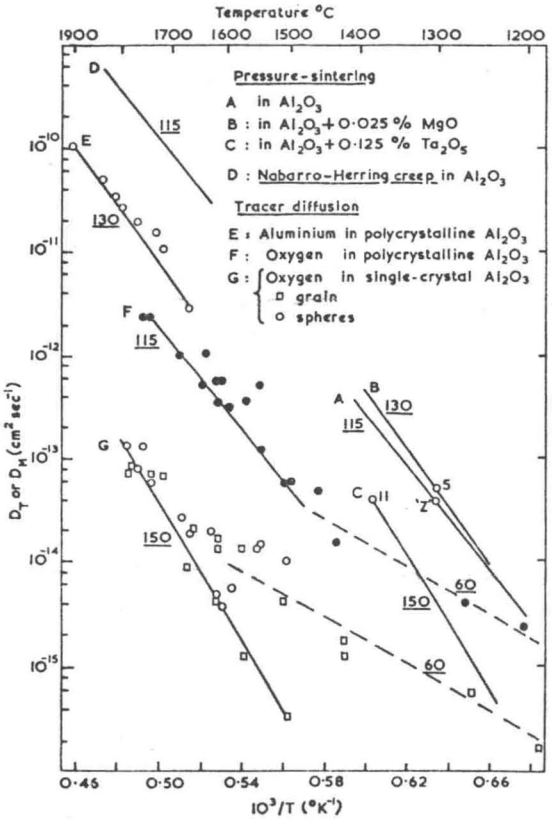

FIGURE 4
Diffusion coefficients in alumina.

with gradients appropriate to the activation energies measured for each type of specimen. The activation energy in kcal.mole^{-1} is shown underlined alongside each plot. Plots A, B and C thus represent the diffusion coefficients measured in all the present pressure-sintering experiments. Plot D on the same figure represents the diffusion coefficients (D_M) for Nabarro–Herring creep in polycrystalline alumina (sintered Linde A), recalculated from the results of HEWSON and KINGERY[5] using the modified Nabarro–Herring creep equation.

$$\dot{\epsilon} = \frac{40}{3}\,\frac{D_M\Omega_s\sigma}{L^2kT}$$

This plot falls very close to the extrapolation of plot A for pressure-sintering in alumina with no added impurity.

6. INTERPRETATION OF THE MEASURED ACTIVATION ENERGIES

The three activation energies determined in the present work (115, 130 and 150 kcal.mole^{-1} approximately) have all been quoted in the literature from time to time in connection with sintering or creep in alumina (Table 5).

Table 5

Experiment	*Activation energy* (kcal.mole^{-1})	*Reference*
Initial sintering (various aluminas)	142–150	JOHNSON and CUTLER[6]
Neck growth of spheres	131	KUCZYNSKI[7]
Grain growth	153	COBLE[8]
Sintering shrinkage	150	COBLE[8]
Sintering shrinkage	150	BRUCH[9]
Nabarro–Herring creep	~115	HEWSON and KINGERY[5]
Nabarro–Herring creep	~130	WARSHAW and NORTON[3]
Nabarro–Herring creep	~130	FOLWEILER[4]

In addition, PALADINO and KINGERY[10] measured an activation energy of 114 ± 15 kcal.mole^{-1} for aluminium tracer diffusion in polycrystalline alumina: and OISHI and KINGERY[11] observed three different activation energies for oxygen tracer diffusion in alumina: namely 110 ± 15 kcal.mole^{-1} with polycrystalline material, 152 ± 25 kcal.mole^{-1} with single crystals, and very approximately 60 kcal.mole^{-1} at lower temperatures with both types of sample. The experimental points for these tracer experiments are plotted in Figure 4.

Interpretation of the activation energy values measured in the present work, in terms of the published values for tracer diffusion, requires a theoretical analysis of the range of possible activation energies for diffusion observable in alumina.

6.1 The Theoretical Activation Energies for Ionic Diffusion in Alumina

The corundum lattice consists of oxygen ions arranged in nearly hexagonal close packing with aluminium ions filling two-thirds of the octahedral interstices. It is thus

improbable that oxygen ions take up interstitial positions, which means that the oxygen vacancies required for sintering or for oxygen tracer diffusion can exist only if Schottky defects are present. (A Schottky defect will be defined as an electrically neutral group of vacancies comprising two aluminium and three oxygen vacancies).

The thermodynamic theory of vacancy equilibrium, as discussed in textbooks on the subject,[12] predicts that, in the case of alumina:

$$(N_{va})^3\,(N_{vc})^2 = \exp\{-Q_s/RT\} \quad . \quad (7)$$

where N_{va} is the equilibrium fraction of vacant anion sites, N_{vc} is the equilibrium fraction of vacant cation sites, and Q_s is the molar free energy of formation of a complete Schottky defect. The equation is valid provided that both types of vacancy are free to distribute themselves randomly within the lattice.

The diffusion coefficient appropriate to a given species of ion is proportional to the vacancy concentration for that species multiplied by a Boltzmann term containing the activation energy for movement, that is:

for anions,

$$D = k_1 N_{va} \exp\{-Q_{ma}/RT\} \quad . \quad . \quad . \quad (8)$$

and for cations,

$$D = k_2 N_{vc} \exp\{-Q_{mc}/RT\} \quad . \quad . \quad . \quad (9)$$

where k_1 and k_2 are constants, and Q_{ma} and Q_{mc} are the molar activation energies for the movement of anion vacancies and cation vacancies respectively.

6.1.1 Pure Crystal

In a crystal of alumina which contains no vacancies arising because of the presence of impurities, the equation

$$2N_{va} = 3N_{vc}$$

must be satisfied, to maintain overall charge neutrality within the crystal. Combining this equation with Equation (7), one obtains

$$N_{va} = 1{\cdot}18 \exp\{-Q_s/5RT\}$$

and

$$N_{vc} = 0{\cdot}784 \exp\{-Q_s/5RT\}$$

Substituting these values of N_{va} and N_{vc} into Equations (8) and (9), one obtains the two intrinsic diffusion coefficients

$$D_a = 1{\cdot}18\, k_1 \exp\{-(Q_s/5 + Q_{ma})/RT\} \quad . \quad (10)$$

and

$$D_c = 0{\cdot}784\, k_2 \exp\{-(Q_s/5 + Q_{mc})/RT\} \quad . \quad (11)$$

6.1.2 Crystal Containing a Fixed Minimum Concentration of Cation Vacancies

If an alumina crystal contains only either a concentration of a cationic impurity with a valency greater than that of aluminium or a concentration of an anionic impurity with a valency less than that of oxygen (e.g. halide ions), then (neglecting the possibility of interstitial anions) there will exist within the lattice a sufficient concentration of cation vacancies to neutralize the excess positive charge caused by the presence of the impurity. If the impurity concentration is low, and the temperature is sufficiently high that the number of vacancies arising for thermodynamic reasons greatly exceeds the number required to neutralise the impurity ions, then the intrinsic diffusion coefficients derived in the last section will be appropriate. At lower temperatures, however, or in the presence of appreciable amounts of impurity, the concentration of cation vacancies may be considered constant, being of magnitude just sufficient to neutralize the impurity ions, and different diffusion coefficients will be observed.

Equation (7) is assumed to be valid under all conditions, and may now be written

$$(N_{va})^3\,(C_c)^2 = \exp\{-Q_s/RT\}$$

where C_c is the constant cation vacancy concentration.

Hence

$$N_{vc} = C_c$$

and

$$N_{va} = C_c^{-\frac{1}{2}} \exp\{-Q_s/3RT\}$$

Substituting these values into Equations (8) and (9) results in the two extrinsic diffusion coefficients:

$$D_{a1} = k_1 C_c^{-\frac{1}{2}} \exp\{-(Q_s/3 + Q_{ma})/RT\} \quad . \quad (12)$$

and

$$D_{c1} = k_2 C_c \exp\{-Q_{mc}/RT\} \quad . \quad . \quad . \quad (13)$$

which will be referred to as the "extrinsic, class 1" coefficients henceforward. It has been assumed that the presence of small amounts of impurity has negligible effect on Q_{ma} and Q_{mc}.

6.1.3 Crystal Containing a Fixed Minimum Concentration of Anion Vacancies

If an alumina crystal contains monovalent or divalent cation impurities, there will always exist sufficient anion vacancies to neutralize the excess negative charge caused by such impurities. At low temperatures, or in the presence of appreciable amounts of impurity, the concentration of anionic vacancies may be considered constant.

Hence

$$N_{va} = C_a$$

where C_a is the constant anion vacancy concentration.

Modifying Equation (7) accordingly gives:

$$(C_a)^3\,(N_{vc})^2 = \exp\{-Q_s/RT\}$$

Hence

$$N_{vc} = C_a^{-\frac{1}{2}} \exp\{-Q_s/2RT\}$$

and substitution into Equations (8) and (9) results in two further extrinsic diffusion coefficients

$$D_{a2} = k_1 C_a \exp\{-Q_{ma}/RT\} \quad . \quad . \quad . \quad (14)$$

and

$$D_{c2} = k_2 C_a^{-3} \exp\{-(Q_s/2 + Q_{mc})/RT\} \quad . \quad (15)$$

which will be referred to as the "extrinsic, class 2" coefficients.

6.1.4 The Six Activation Energies

From Equations (10) to (15) it is seen that there are six possible activation energies which may be observed

for ionic diffusion in alumina:

$$\left.\begin{aligned} Q_a &= Q_s/5 + Q_{ma} \\ Q_c &= Q_s/5 + Q_{mc} \end{aligned}\right\} \text{Intrinsic}$$

$$\left.\begin{aligned} Q_{a1} &= Q_s/3 + Q_{ma} \\ Q_{c1} &= Q_{mc} \end{aligned}\right\} \text{Extrinsic, class 1 (excess cation vacancies)}$$

$$\left.\begin{aligned} Q_{a2} &= Q_{ma} \\ Q_{c2} &= Q_s/2 + Q_{mc} \end{aligned}\right\} \text{Extrinsic, class 2 (excess anion vacancies)}$$

6.2 Discussion

During the present work, the impurities added to alumina in various experiments were magnesia and tantalum pentoxide. The likely effect of adding each of these impurities will now be considered.

When magnesia enters the corundum lattice, either two Mg^{2+} ions will replace two Al^{3+} ions with the formation of an oxygen vacancy, or else three Mg^{2+} ions will replace two Al^{3+} ions with the third Mg^{2+} ion being accommodated in a spare octahedral lattice site. In the second instance the equilibrium vacancy concentration would not be expected to be different from that in an undoped crystal, and no difference in diffusion kinetics would be expected. The present work has shown that the introduction of magnesia into alumina markedly alters the activation energy observed in pressure-sintering, so that it would appear that the first of the above alternatives is correct and thus that a high fixed minimum concentration of anion vacancies will exist in magnesia-doped alumina. The concentration of cation vacancies must be simultaneously suppressed (to maintain the equilibrium of Equation (7)) so that the cations will be the less mobile species, and the observed activation energy (~ 130 kcal.mole^{-1}) must be the extrinsic (class 2) cation activation energy, Q_{c2}.

In alumina containing tantalum, the only likely mechanism is that three Ta^{5+} ions must replace five Al^{3+} ions, with the formation of two aluminium ion vacancies. Any other alternative would require the introduction of oxygen ions into interstitial positions, which is most unlikely because alumina consists basically of a close-packed oxygen lattice. Tantalum-doped alumina may thus be expected to contain a high fixed minimum concentration of cation vacancies and the sintering process will probably be controlled by the depressed concentration of anion vacancies. The observed activation energy for pressure-sintering in tantalum-doped alumina (~ 150 kcal.mole^{-1}) will thus be expected to be the extrinsic (class 1) anion activation energy, Q_{a1}.

Inspection of the set of equations representing the six possible diffusional activation energies in alumina indicates that

$$Q_{a1} > Q_a > Q_{a2}$$

and

$$Q_{c2} > Q_c > Q_{c1}$$

The activation energy for pressure-sintering in undoped alumina (~ 115 kcal.mole^{-1}) is lower than either of the other two observed energies (believed to be Q_{a1} and Q_{c2}), and so is likely to be one of the intrinsic activation energies Q_a or Q_c, depending on whether the anions or the cations are the less mobile.

The full set of six activation energies will now be calculated from the values

$$Q_{c2} = 130 \pm 3$$

$$Q_{a1} = 150 \pm 5$$

$$Q_a \text{ or } Q_c = 115 \pm 4$$

The equations for the six activation energies can be arranged to give the following relationships:

$$Q_a = Q_{a1} - \frac{4}{9}(Q_{c2} - Q_c)$$

$$Q_c = Q_{c2} - \frac{9}{4}(Q_{a1} - Q_a)$$

$$Q_{ma} = \frac{5}{2}Q_a - \frac{3}{2}Q_{a1} = Q_{a1} - \frac{10}{9}(Q_{c2} - Q_c)$$

$$Q_{mc} = Q_{c2} - \frac{15}{4}(Q_{a1} - Q_a) = \frac{5}{2}Q_c - \frac{2}{3}Q_{c2}$$

$$Q_s = \frac{15}{2}(Q_{a1} - Q_a) = \frac{10}{3}(Q_{c2} - Q_c)$$

In the case where $Q_a = 115 \pm 4$, these equations give the following set of values:

$$Q_a = 115 \pm 4$$
$$Q_c = 51 \pm 23$$
$$Q_{a1} = 150 \pm 5$$
$$Q_{c1} = Q_{mc} = < 36$$
$$Q_{a2} = Q_{ma} = 63 \pm 17$$
$$Q_{c2} = 130 \pm 3$$
$$Q_s = 262 \pm 68$$

Alternatively, if $Q_c = 115 \pm 4$, the following values are obtained:

$$Q_a = 143 \pm 8$$
$$Q_c = 115 \pm 4$$
$$Q_{a1} = 150 \pm 5$$
$$Q_{c1} = Q_{mc} = 105 \pm 9$$
$$Q_{a2} = Q_{ma} = 133 \pm 13$$
$$Q_{c2} = 130 \pm 3$$
$$Q_s = 50 \pm 23$$

The second of the above sets of values seems unlikely to be correct for two reasons. Firstly, it is predicted that no experimentally observable activation energy of less than about 100 kcal.mole^{-1} is possible, whereas OISHI and KINGERY[11] observed an activation energy of roughly 60 kcal.mole^{-1} for oxygen tracer diffusion at lower temperatures ($\lesssim 1450$ C). Secondly, $Q_s \simeq 50$ kcal.mole^{-1} seems very low for the formation energy of a Schottky defect containing five vacancies. It would mean that the formation energy per vacancy was only about half that determined for vacancies in sodium chloride.[13]

The first set of values, determined assuming that $Q_a = 115 \pm 4$, appears to be more satisfactory. $Q_s \simeq 260$ kcal.mole^{-1}, so that the formation energy per vacancy is about twice that determined for sodium chloride. In addition, the three anion activation energies (150 ± 5, 115 ± 4 and 63 ± 17 kcal.mole^{-1}) correspond closely to

the three values determined for anion tracer diffusion by Oishi and Kingery (152 ± 25, 110 ± 15 and about 60 kcal.mole^{-1} respectively). If this set of values is accepted, the following conclusions must be drawn:

(1) Paladino and Kingery's value for cation tracer diffusion in polycrystalline alumina (114 ± 15 kcal.mole^{-1}) must represent extrinsic cation diffusion in the presence of excess oxygen vacancies ($Q_{c2} = 130 \pm 3$ kcal.mole^{-1}),

(2) Oishi and Kingery's value for anion tracer diffusion in polycrystalline alumina (110 ± 15 kcal.mole^{-1}) represents intrinsic oxygen diffusion ($Q_a = 115 \pm 4$ kcal.mole^{-1}),

(3) Oishi and Kingery's value for anion tracer diffusion in single-crystal alumina (152 ± 25 kcal.mole^{-1}) represents extrinsic anion diffusion in the presence of excess cation vacancies ($Q_{a1} = 150 \pm 5$ kcal.mole^{-1}), and

(4) their observed lower-temperature value for anion tracer diffusion in both types of sample (about 60 kcal.mole^{-1}) represents extrinsic anion diffusion in the presence of a fixed concentration of anion vacancies ($Q_{ma} = 63 \pm 17$ kcal.mole^{-1}).

In Figure 4, lines with gradients appropriate to the calculated activation energies are superimposed on the experimental data for tracer diffusion. It is seen that a good fit is obtained in all cases.

It must be remembered that the calculations in this section have been made assuming that the vacancy concentrations in alumina are predicted by the conventional thermodynamic theory of Schottky defects, that the changes in activation energy brought about in the pressure-sintering experiments are caused by the introduction of extrinsic vacancy concentrations in the manner suggested, and for no other reason, and that the activation energies for the movement of the ionic species are essentially unaffected by the presence of small amounts of impurity. The way in which it has been found possible to correlate the calculated values with published results for tracer diffusion lends some confidence to the calculations.

The conclusion that the activation energy for aluminium ion diffusion in polycrystalline alumina observed by Paladino and Kingery (114 ± 15 kcal.mole^{-1}) was that for extrinsic cation diffusion in the presence of excess oxygen vacancies could presumably be checked by aluminium tracer measurements using alumina doped in such a way as to induce an excess concentration of cation vacancies, when a low activation energy (< 36 kcal.mole^{-1}) should be observed, according to the present calculations.

The conclusions concerning the meaning of the diffusion coefficients measured by anionic tracer diffusion lead to some interesting speculations. According to OISHI and KINGERY,[11] there was definite evidence that the observed anion tracer diffusion in their polycrystalline samples took place by grain-boundary diffusion (argued from the observation that the apparent diffusion coefficient decreased with time, i.e. with depth of penetration from the surface). If this is so, the implication is that intrinsic oxygen diffusion occurred in grain-boundary regions. However, extrinsic (class 1) diffusion was observed for their single-crystal samples, with diffusion coefficients at least an order of magnitude lower than for intrinsic diffusion. It is probable that diffusion within the grains of the polycrystalline samples would follow the same mechanism as that within the single-crystal samples, so that an immediate explanation is obtained for the preferential grain-boundary diffusion in the polycrystals.

That intrinsic diffusion was observed in grain-boundary regions implies either that the trace impurities giving rise to excess cation vacancies were repelled from the grain boundaries, or that these impurity ions associated with dislocations in the boundary regions so that they no longer caused anomalous vacancy concentrations (being no longer free to distribute themselves randomly within the lattice). The latter suggestion also offers an explanation of why intrinsic ionic diffusion should be observed with undoped alumina in the present pressure-sintering experiments at temperatures below 1400°C, when extrinsic diffusion might be expected. The alumina grains undergoing pressure-sintering are likely to contain high concentrations of dislocations because of the stresses to which they are subjected, and if association readily occurs between trace-impurity ions and dislocations, this could explain why intrinsic diffusion can be observed at such low temperatures.

The calculations in the present section imply that the oxygen tracer diffusion measurements of Oishi and Kingery with single-crystal specimens (Figure 4, plot G) represent extrinsic class 1 diffusion at temperatures above about 1650°C and extrinsic class 2 diffusion at lower temperatures, although some samples exhibited extrinsic class 1 behaviour at temperatures as low as about 1500°C. In particular, samples annealed in air at 1900°C before diffusion coefficients were measured at lower temperatures (below about 1650°C) gave results which indicated extrinsic class 1 behaviour (i.e. the points fell on the 150 kcal.mole^{-1} plot). It might not be expected that a set of samples should exhibit both types of extrinsic diffusion (according to the temperature range) with no evidence of intrinsic diffusion, but it is possible that the samples contained different types of impurities which gave rise to both cation and anion vacancies, in different concentrations. If this is so, the results suggest that, at temperatures above 1650°C, the excess concentration of cation vacancies controlled the diffusion behaviour, while the impurity-controlled concentration of anion vacancies could be ignored at these temperatures. As the temperature was reduced below about 1600°C, it would appear that the concentration of anion vacancies was prevented from falling below the value fixed by the presence of the appropriate impurity ions, so that extrinsic class 2 diffusion was observed. It appears that annealing at high temperature can cause either a reduction in the concentration of these latter impurity ions, or their association with lattice defects such as dislocations, so that extrinsic class 1 diffusion can be extended to lower temperatures. The samples were reported to contain traces of magnesium and calcium (which may cause anion vacancies), silicon (which may cause cation vacancies), and may have contained anionic impurities which were not sought for during analysis.

From Equation 3(a) (where $z_a = 2$ and $z_c = -3$), D_M controlled by oxygen diffusion should be a little more than twice the tracer diffusion coefficient. If the higher-temperature part of plot F in Figure 4 is accepted as representing intrinsic oxygen diffusion, it is seen that

plots A and D (for intrinsic oxygen diffusion in pressure-sintering and in Nabarro–Herring creep) indicate that D_M controlled by intrinsic oxygen diffusion is more than an order of magnitude higher than the tracer diffusion coefficient. This may indicate that the (theoretically calculated) geometrical factor in the Nabarro–Herring creep equation is inaccurate, or may be explained by some other inaccuracy in the calculation of plots A and D, or by inaccuracy in the experimental evaluation of tracer coefficients. In view of the range of possible sources of miscalculation, it may be considered that the observed order-of-magnitude agreement is satisfactory.

Comparison of plots A and B (Figure 4) suggests that D_M (and hence sintering rate) was slightly increased by the addition of 0·025%$_0$ of magnesia, whereas it has usually been noted[5,14] that magnesia tends to reduce sintering or creep rates. These observations are not incompatible, firstly because the diffusion coefficients represented by plots A and B are claimed to be accurate only to within about half an order of magnitude, and secondly because plot B would be depressed to lower values of diffusion coefficients for greater concentrations of magnesia (from Equation (15), D_{c2} is inversely proportional to the impurity concentration to the power 3/2).

ACKNOWLEDGMENT

The Ministry of Technology is thanked for supporting this work.

MS RECEIVED 10/10/1968

REFERENCES

1. FRYER, G.M., *Trans. Brit. Ceram. Soc.*, **68**, (4), 185, 1969
2. FRYER, G.M., *Trans. Brit. Ceram. Soc.*, **68**, (4), 181. 1969
3. WARSHAW, S.I., and NORTON, F.H., *J. Amer. Ceram. Soc.*, **45**, 479, 1962.
4. FOLWEILER, R.C., *J. Appl. Phys.*, **32**, 773, 1961.
5. HEWSON, C.W., and KINGERY, W.D., *J. Amer. Ceram. Soc.*, **50**, 218, 1967.
6. JOHNSON, D.L., and CUTLER, I.B., *J. Amer. Ceram. Soc.*, **46**, 545, 1963.
7. KUCZYNSKI, G.C., ABERNATHY, L., and ALLEN, J., "Kinetics of High-Temperature Processes" (Ed. W.D. Kingery, Wiley, New York, 1959), p.163.
8. COBLE, R.L., *J. Appl. Phys.*, **32**, 793, 1961.
9. BRUCH, C.A., *Amer. Ceram. Soc. Bull.*, **41**, 799, 1962.
10. PALADINO A.E., and KINGERY, W.D., *J. Chem. Phys.*, **37**, 957, 1962.
11. OISHI, Y., and KINGERY, W.D., *J. Chem. Phys.*, **33**, 480, 1960.
12. (a) SHEWMAN, P.G., "Diffusion in Solids" (McGraw-Hill, 1963).
    (b) GIRIFALCO, L.A., "Atomic Migration in Crystals" (Blaisdell, 1964).
13. ETZEL, H.W. and MAURER, R.J., *J. Chem. Phys.*, **18**, 1003, 1950.
14. JORGENSEN, P.J., General Electric Co., Report No. 64–RL–3744M, 1964.